Iranian Journal of Materials Forming 8 (3) (2021) 4-17

Online ISSN: 2383-0042

IJMF

Iranian Journal of Materials Forming

Journal Homepage: http://ijmf.shirazu.ac.ir

Research Article

Hot Deformation Behavior and Development of Constitutive Equations on a Novel γ-γ′ Ni-base Superalloy: AD730

M. Mirzaie[1], G.R. Ebrahimi[2*], H. Ezatpour[3] and S. Aliakbari Sani[1,2]

[1] Materials and Polymers Engineering Department, Faculty of Engineering, Hakim Sabzevari University, Sabzevar, Iran
[2] Materials and Metallurgical Engineering Department, Faculty of Engineering, Ferdowsi University of Mashhad, Mashhad, Iran
[3] Department of Engineering Sciences, Hakim Sabzevari University, Sabzevar, Iran

ARTICLE INFO

Article history:

Received 16 March 2021
Reviewed 22 March 2021
Revised 11 April 2021
Accepted 25 April 2021

Keywords:

AD730
Hot deformation
DRX
Hyperbolic sine modeling
γ′ phase

ABSTRACT

In this work, hot deformation behavior and microstructural evolution for a novel Ni-base superalloy, AD730, were analyzed using a hyperbolic sine constitutive equation. The hot compression tests were carried out at a wide range of temperatures (950ºC-1200ºC) and strain rates (0.001-1 s^{-1}). The modeling was done at the overall deformation conditions, and then the obtained important constitutive parameters, i.e., n and Q, were calculated to be 5.44 and 820.26 kJ/mol, respectively. Microstructural evolution showed two distinct domains at higher temperatures (1100ºC, 1150ºC, and 1200ºC) and lower ones (950ºC, 1000ºC, and 1050ºC) accomplished by dynamic recrystallization (DRX) and non-DRX behavior due to absence and presence of γ′ particles, respectively. Furthermore, the constitutive equations were analyzed based on both separated temperature domains. The obtained parameters from this approach demonstrated better results as compared with the literature, i.e., the parameters of n and Q were calculated to be 8.60 and 1160.45 kJ/mol at the lower domain, in contrast with 3.69 and 468.32 kJ/mol which were at higher ones. Additionally, the stress prediction data based on correlation coefficient factor (R^2) presented the best reliable prospective at two separated domains as 0.994, as compared with overall conditions prediction with 0.963. It was found that hot working of AD730 alloy as well as flow stress can be essentially affected by the γ′-phase. Therefore, the hot deformation behavior of AD730, as a γ′-containing superalloy, should be performed at identified domains considering the solution temperature of γ′-phase.

1. Introduction

Nickel-based superalloys exhibit high strength and excellent corrosion resistance, as well as relatively elevated temperatures. These qualities make them high-demanded material in various industries and are extensively applied during the manufacturing of key components in the gas turbines, blades, discs, and shafts. Generally, most high-temperature parts within a gas turbine are manufactured by using a wrought type which is typically made by cast-to-wrought conversion known specifically in heavy industries [1, 2]. It is noted that the microstructure and mechanical properties of Ni-based superalloys depend on γ′ precipitates and grain structure are controlled by heat and thermo-mechanical treatments; respectively [1, 3]. Hence, it is

* Corresponding author
E-mail address: r.ebrahimi@um.ac.ir (G.R. Ebrahimi)
https://doi.org/10.22099/ijmf.2021.40096.1179

vital to study the hot deformation behaviors and microstructural evolution of nickel-based superalloys during thermo-mechanical treatment.

Material flow behavior in the process of hot deformation is included in the hardening and softening mechanism such as work hardening, dynamic recovery (DRV), dynamic recrystallization (DRX), dynamic precipitation (DP), and strain-induced precipitation (SIP). These mechanisms have an important impact on metallurgical and mechanical properties including flow stress and microstructure [4-6]. The predictions of stress and simulation of hot deformation process have found great prominence in industrial point of view, particularly for novel alloys. To investigate the material flow behavior, hot compression tests, hot tensile tests, and hot torsion tests are usually done. Arrhenius type equations are popular and widely used in the prediction of material flow behavior [1]. They have been generally used to pronounce the relationships between flow stress (σ), deformation temperature (T), and strain rate ($\dot{\varepsilon}$) as following [5, 7-9]:

$$\dot{\varepsilon}\exp(-\mathrm{Q}/RT) = \mathrm{A}[\sinh(\alpha\sigma)]^{\mathrm{n}} \quad (1)$$

$$\dot{\varepsilon}\exp(-\mathrm{Q}/RT) = \mathrm{B}\sigma^{n_1} \quad (2)$$

$$\dot{\varepsilon}\exp(-\mathrm{Q}/RT) = \mathrm{C}\exp(\beta\sigma) \quad (3)$$

where, the A, B, C, n_1, β, α, and R are material constants. Q denotes activation energy and n is the stress power. Furthermore, the power-law equations Eq. (2) and exponential equations Eq. (3) are adopted for low stress ($\alpha\sigma$<0.8) and high stress ($\alpha\sigma$ >1.2), respectively; however, the hyperbolic sine constitutive equation Eq. (1) is usually employed for all stress levels, as an appropriate alternative approach. Furthermore, the effects of strain rate and temperature can be represented by the Zener-Holloman parameter (Z) as follows:

$$\mathrm{Z} = \dot{\varepsilon}\exp(-\mathrm{Q}/RT) \quad (4)$$

Although, hot deformation parameters such as temperature and strain rate can lead to a thermo-mechanical process of superalloys [10, 11], but, correlating microstructure and metallurgical properties can be considered as a very effective paradigm. It was shown that the hot tensile behavior of Incoloy 901 superalloy has better workability due to easier DRX progress facilitated by smaller initial grains, as compared to as-cast ones [12]. It was reported [13] that the hot deformation of cast-U720 alloy with two various grain structures i.e., equiaxed and columnar types are different. Likewise, it was observed [14] that the hot deformation of γ′-free U720 alloy with the coarse structure is accompanied by more DRX as compared with fine grain-structure type containing fine γ′-intermetallic particles that repress the DRX progress in the microstructure. It was suggested [15, 16] that thermal twins facilitate recrystallization during and after hot deformation. Similarly, the second phase in superalloys has amazing effects on hot deformation which depends on their size, volume fraction, morphology, and intrinsic properties. It has been proven [17-20] that hot deformation of In718 and derivatives superalloys can be controlled by the progress of the DRX phenomena via particle stimulated nucleation (PSN) mechanism which is affected by delta (δ) precipitates. Additionally, it was showed [21-23] that the MC-carbides can improve workability with the encouragement of DRX with the PSN mechanism. On the other hand, for the hardenable superalloys, the fine γ′ particles can suppress the softening phenomena with their Zener-drag effect [22, 24].

Recently, AD730 alloy, the novel wrought nickel-based superalloy which was developed by Aubert & Duvel Company, has been designed to enhance the properties of complex parts used in turbine engines over 700°C. It has been reported [25, 26] that its high-temperature mechanical properties are comparable with the well-known nickel superalloy classes such as Udimet 720 and Waspaloy. AD730 alloy strengthened by ordered γ′ precipitates, $L1_2$ structure, with almost volume fraction of 37% at 700 °C [26], which coexists coherently with matrix, γ phase. This alloy can be easily deformed from the cast-to-wrought changing condition by conventional hot deformation routes such as hot forging and hot rolling [25]. To develop appropriate

wrought AD730 alloy within the cogging process, it is necessary to understand the hot deformation behavior. In this work, the hot deformation behavior of ingot AD730 alloy was studied at the temperature range of 950ºC - 1200ºC and strain rate range of 0.001-1 s^{-1}, separated into two regions of higher and lower domains. In addition, to describe the hot working behavior during thermo-mechanical processing, flow stress curve was predicted based on hyperbolic sine constitutive equations.

2. Materials and Methods

AD730 alloy with chemical composition of 2.0Al-2.7Ti-2.8W-0.98Nb-3.0Mo-14.5Cr-9.8Co-4.8Fe-0.043C-0.008B (wt.%) was melted in a vacuum induction melting (VIM) furnace under 10^{-3} bar pressure and then poured into a ceramic mold. The cast specimen was homogenized at 1200 °C through 100 min followed by water quenching. As illustrated in Fig. 1(a), the coarse grain structure of the cast-homogenized sample, about 0.5-2 mm in diameter was measured as starting material. Based on the DTA result during the cooling route using BAHR GmbH, the precipitation temperature was obtained 1079°C (Fig. 1(b)). The cylindrical hot compression specimens were machined out from homogenized specimens by wire-cut discharge machine with a size of 12 mm in height and 8 mm in diameter. A Zwick/Roell Z250 testing machine equipped with a controlled furnace was used to carry out the tests in a temperature range of 950-1200 °C and strain rates of 0.001-1 s^{-1} up to the strain of 0.5. The soaking time specimens were held at the test temperature for 5 min before hot compression took place and quenched immediately after test completion. Optical microscopy as well as field emission gun scanning electron microscopy (FEG-SEM) were employed to examine the obtained microstructure. Finally, the Image J software was used to calculate the grain size.

3. Results and Discussions

3.1. Flow curves analysis

All the flow curves of the investigated alloy are shown in Fig. 2. In each of the curves, the flow stress was

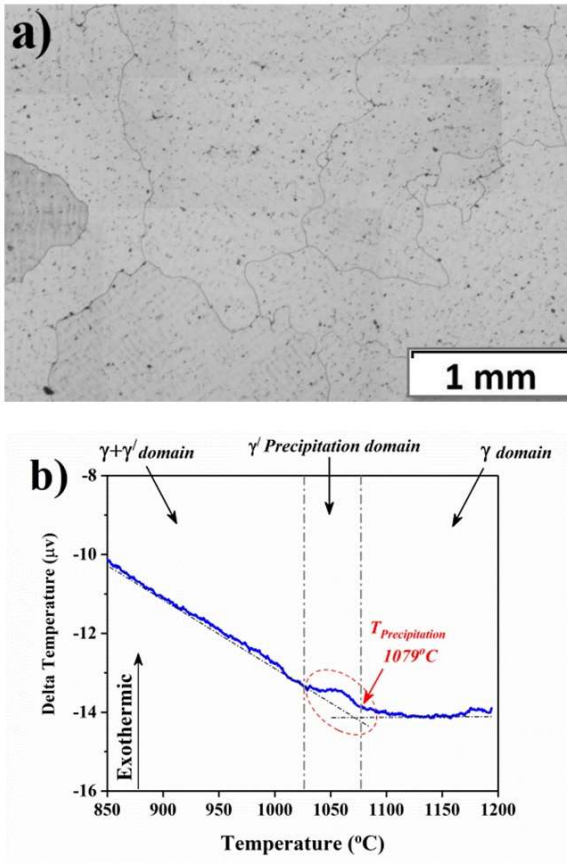

Fig. 1. a) Optical microstructure and b) DTA results during the cooling route of the cast-homogenized alloy.

increased to peak point related to the work hardening due to the generation of dislocations and their further interactions [4, 6]; however, it is continuously decreased by the occurrence of work softening that can be commenced by dynamic recrystallization or flow localization [22, 27]. It can be seen that the flow stresses decline with a decrease in strain rate and an increasing temperature that is associated with more flow softening. Furthermore, the flow stresses at lower temperatures domains (950-1050°C) were generally much higher than ones of 1100-1200°C.

3.2. Constitutive equation analysis

To model the hot deformation of AD730 superalloy, the constitutive equation was taken into account in all conditions, the temperatures of 950-1200°C and strain rates of 0.001-1 s^{-1}, at the final strain of 0.5. The β value from Eq. (2) and n_1 value from Eq. (3) was obtained 0.05507 and 8.431 from average slopes of curves in $\ln\dot{\varepsilon}$

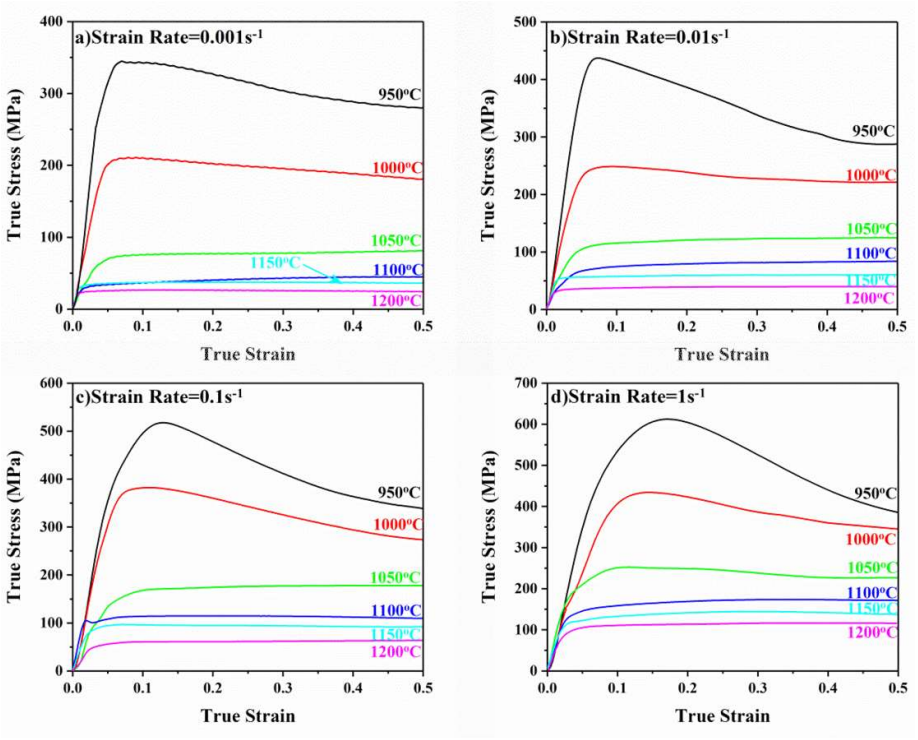

Fig. 2. The experimental flow curves of the AD730 superalloy at different temperatures and strain rates of: a) 0.001 s^{-1}, b) 0.01 s^{-1}, c) 0.1 s^{-1} and d) 1 s^{-1}.

versus σ and $\ln\dot{\varepsilon}$ versus $\ln\sigma$, respectively; as shown in Fig. 3. Then, the α parameter can be obtained 0.006532, as $\alpha = \beta/n_1$ relation [9]. By taking natural logarithms of both sides of Eq. (1), can be rewritten as:

$$\ln\dot{\varepsilon} = n\ln[\sinh(\alpha\sigma)] - (Q/RT) + \ln A \qquad (5)$$

According to Eq. (5), the n-value can be derived from average slopes of $\ln\dot{\varepsilon}$ versus $\ln[\sinh(\alpha\sigma)]$ at each constant temperature (Eq. (6)) as shown in Fig. 3(c) for the investigated alloy. Also, the value of Q is calculated from $\ln[\sinh(\alpha\sigma)]$ versus 1000/RT plots at constant strain rate (Eq. (7)) as presented in Fig. 3(d) for AD730 superalloy. Therefore, the n and Q values for the overall condition are obtained to be 5.44 and 820.3 kJ/mol, respectively.

$$n = \left[\frac{\partial\ln\dot{\varepsilon}}{\partial\ln[\sinh(\alpha\sigma)]}\right]_T \qquad (6)$$

$$Q = \left[\frac{\partial\ln[\sinh(\alpha\sigma)]}{\partial(1000/RT)}\right]_{\dot{\varepsilon}} \qquad (7)$$

It is noteworthy to mention that the obtained Q-value at overall condition for AD730 (820.3 kJ/mol) is significantly greater than the activation energy for self-diffusion of the Nickel element (275 kJ/mol [28]), and the activation energy for Al-diffusion (269 kJ/mol [23]), Ti-diffusion (256 kJ/mol [23]) and Cr-diffusion (278 kJ/mol [29]) into the Ni-matrix. Additionally, the activation energy of the AD730 is higher than other superalloys, i.e., In625 (483 kJ/mol) [30], In718 (467 kJ/mol) [19], and also a novel Ni-based superalloy (420–490 kJ/mol) [31]. This difference demonstrates that the distinct mechanism is active in the presented alloy as compared with other alloys discussed in section 3.4. Fig. 3(d) shows the plot of $\ln Z$ v.s. $\ln[\sinh(\alpha\sigma_{0.5})]$ that its correlation coefficient (R^2) is 0.969. This reveals that the hyperbolic sine equation illustrates a good correlation between stress and thermo-mechanical parameters; however, it does not exhibit the excellent relationship at

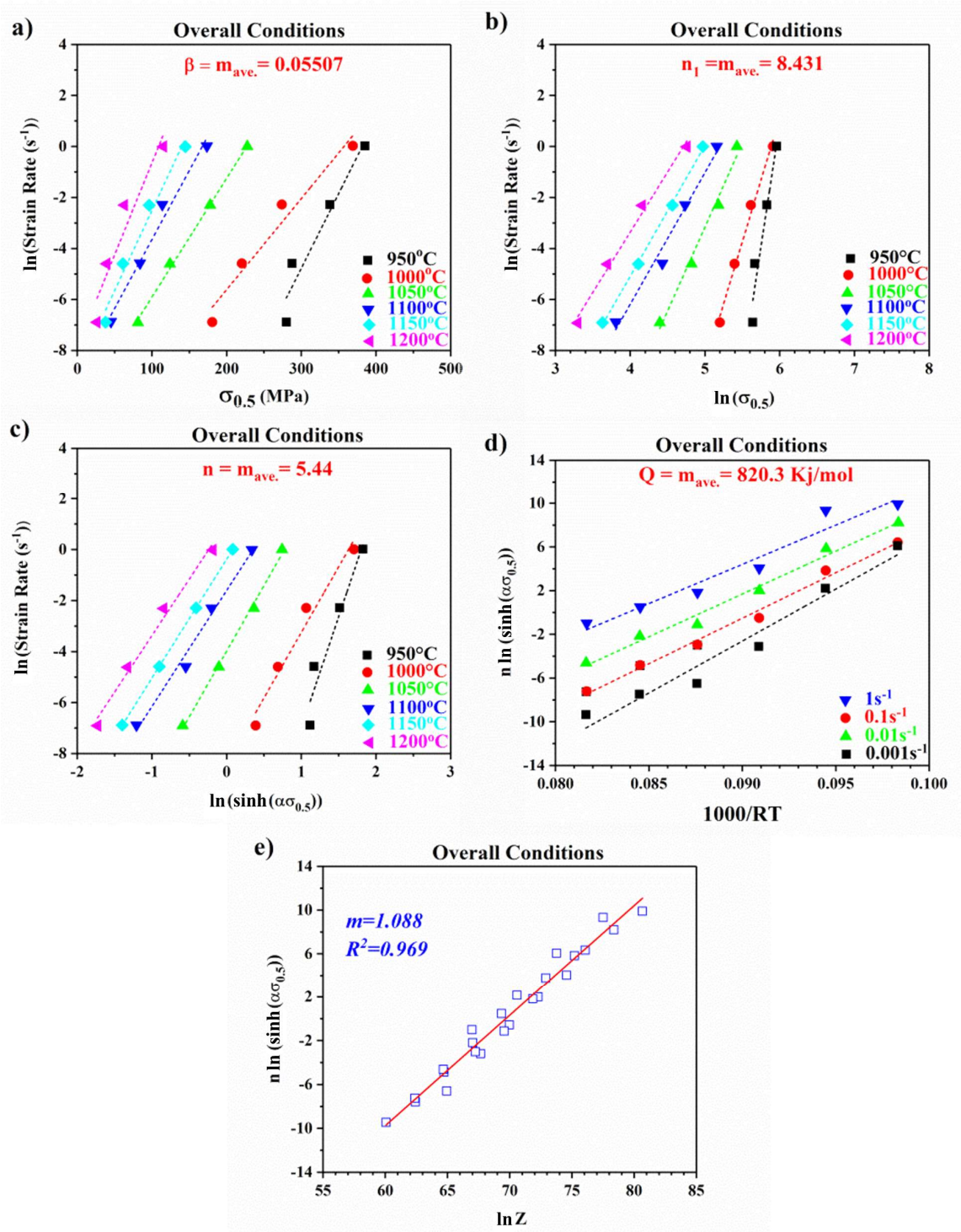

Fig. 3. The variations of a) $\ln\dot{\varepsilon} - \sigma$, b) $\ln\dot{\varepsilon} - \sigma$, c) $\ln\dot{\varepsilon} - \ln(\sinh(\alpha\sigma_{0.5}))$, d) n ln $(\sinh(\alpha\sigma_{0.5})) - 1000/RT$, e) n ln $(\sinh(\alpha\sigma_{0.5})) - \ln Z$ based on hot compression tests at the overall condition.

overall condition (950-1200ºC). According to the reported results, the constitutive equation for AD730 alloy in overall deformation conditions is developed by using the following formula:

$$Z = \dot{\varepsilon}\exp\left(\frac{820259}{8.314T}\right) = (1.83 \times 10^{30})\ln[\sinh(0.006532\sigma)^{5.44}] \quad (8)$$

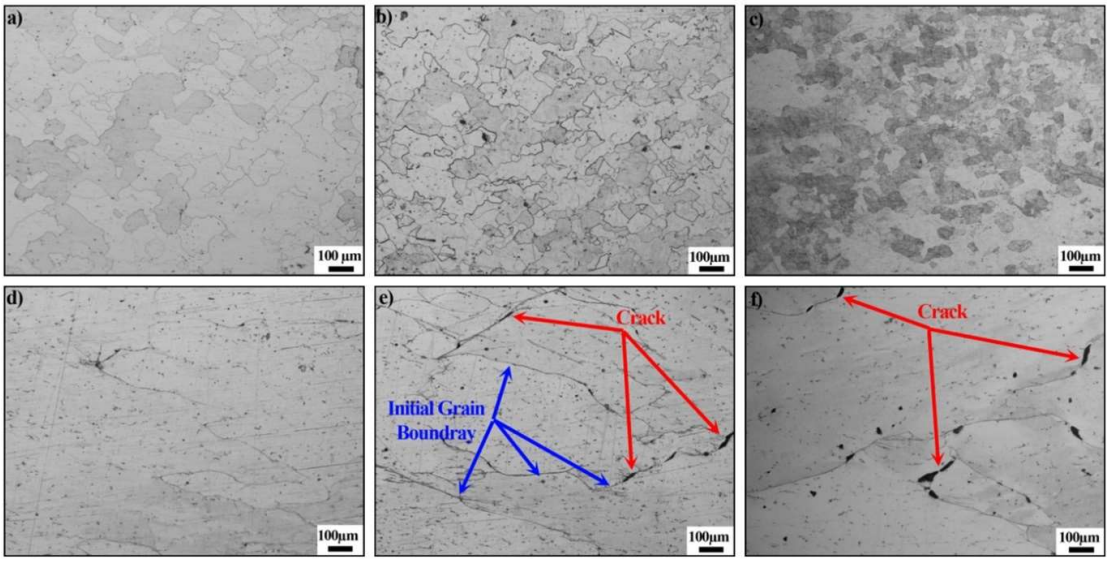

Fig. 4. The hot deformed microstructures at a strain rate of 0.001 s^{-1} and temperatures of a) 1200°C, b) 1150°C, c) 1100°C, d) 1050°C, e) 1000°C, f) 950°C.

3.3. Microstructure observation

The deformed microstructures of AD730 alloy at all temperatures and strain rates of 0.001 s^{-1} are shown in Fig. 4. Fig. 4 (a-c) shows that recrystallized grains nucleated on the as-cast grain boundaries. The type of DRX in this alloy is recognized as the discontinuous type with two separated stages of nucleation and growth [4]. Similarly, the deformed microstructures at the strain rate of 1 s^{-1} presented in Fig. 5(a-c), reveal the same manner in the microstructural evolution and related softening phenomena. Whereas, by comparing Fig. 4 and Fig. 5, the DRXed grains size is raised by the increasing temperature at each constant strain rate, e.g., the DRXed grain size is 38.88 µm (1100°C), 46.79 µm (1150 °C) and 73.6 µm (1200°C) at the strain rate of 1 s^{-1}. Similarly, the size of the DRXed-grain is increased with a decrease in strain rate at each temperature as 63.05 µm at 0.001 s^{-1} to 46.79 µm at 1 s^{-1} for deformation temperature of 1150 °C. These are attributed to the progression of DRX phenomena depending on deformation conditions. Conversely, in lower temperatures, i.e., 1050 °C, 1000 °C, and 950 °C, it can

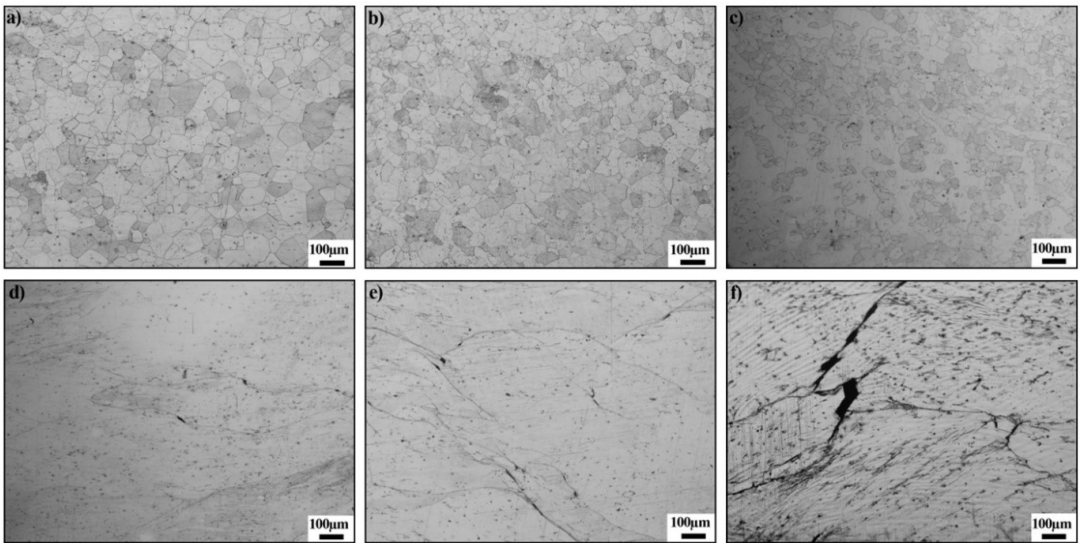

Fig. 5. The hot deformed microstructures at a strain rate of 1s^{-1} and temperatures of a) 1200°C, b) 1150°C, c) 1100°C, d) 1050°C, e) 1000°C, f) 950°C.

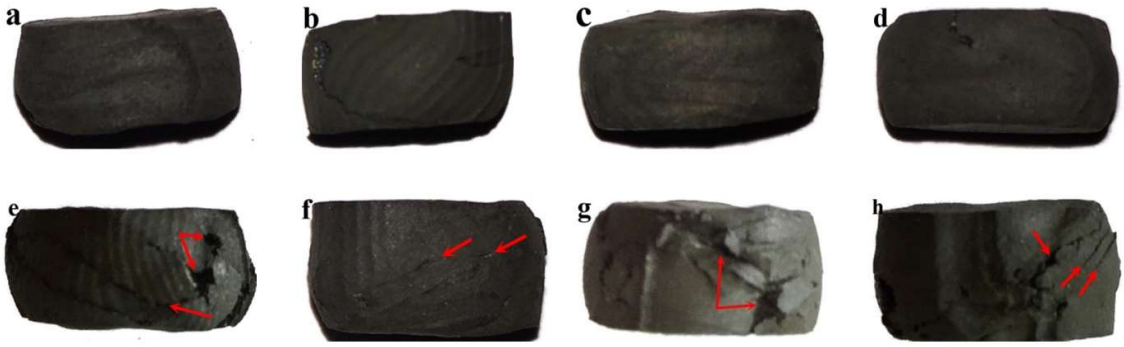

Fig. 6. The images of deformed samples at a) 1200°C-0.001 s^{-1}, b) 1200°C-1 s^{-1}, c) 1100°C-0.001 s^{-1}, d) 1100°C-1 s^{-1}, e) 1050°C-0.001 s^{-1}, f) 1050°C-1 s^{-1}, g) 950°C-0.001 s^{-1}, h) 950°C-1 s^{-1}.

be demonstrated that large deformed grains are observed along with some inter-granular cracks and strain localization indicating the non-presence of any DRX evidence within the mentioned temperature domain. In other words, it is revealed that the two opposite manners, i.e., DRX and non DRX occurred at higher and lower temperature domains, respectively. The images of deformed specimens at various conditions presented in Fig. 6 show the uniform deformation pattern at 1200°C and 1100°C, as a higher temperature domain. In contrast, non-uniform deformation, macro-crack, shear banding, and distortion can be seen at 950°C and 1050°C.

To study in detail, the FE-SEM microstructures of cylindrical samples, holding at deformation temperature for 5 min, at 950°C, 1000°C, 1050°C, and 1150°C are presented in Fig. 7. As can be seen, the large volume fraction of fine γ' precipitations is formed in lower temperatures, while those are not seen in the microstructure of a higher temperature (1150°C). This evidence is interpreted with precipitation temperature of γ' precipitations, 1079°C, extracted from DTA-analysis results. According to obtained results the changes in both flow curves and microstructure can be attributed to the effects of γ' precipitations as the presence of γ' prevent the DRX and the solution of γ'-particles trigger the DRX within microstructure as well decreasing stress level.

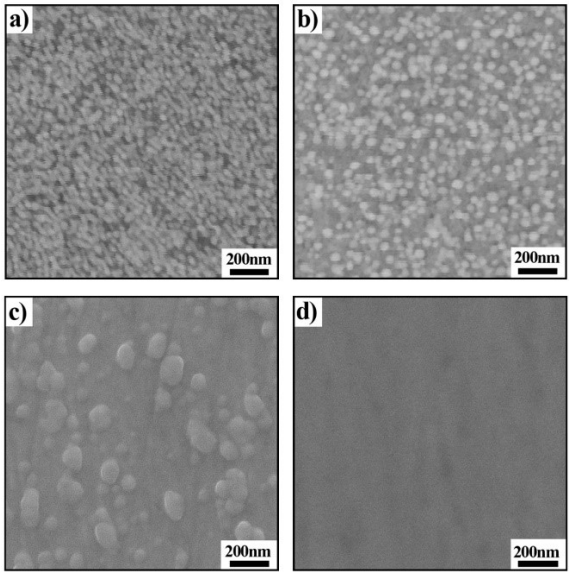

Fig. 7. FESEM microstructures of samples after heating and holding at deformation temperature for 5 min, just before hot compression tests at temperatures of a) 950°C, b) 1000°C, c) 1050°C and d) 1100°C.

3.4. Constitutive analysis at both lower and higher temperature domains

According to the previous section, the hot deformation behavior and the modeling of AD730 alloy are studied in two separate domains, lower and higher ones. Similar to the described approach of section 3.2, the hyperbolic sine equation parameters (n and Q) can be obtained at both domains, as shown in Fig. 8. It is shown that the n and Q values were calculated for the lower region that are 8.60 and 1160.45 kJ/mol, respectively. Nevertheless, the values of 3.69 and 468.32 kJ/mol are calculated for the higher ones. Moreover, the variations of $n \ln(\sinh(\alpha\sigma_{0.5})) - \ln Z$ are shown in Fig. 8(d) which clearly indicates the appropriate modeling at each domain for hot working of AD730 superalloy. The constitutive equations developed at separated domains are expressed in the following formulas:

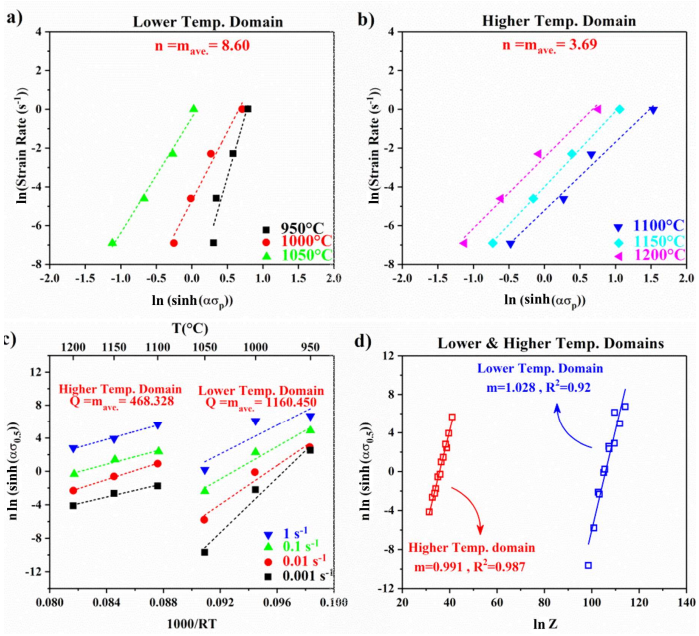

Fig. 8. The variations of $\ln\dot{\varepsilon} - \ln(\sinh(\alpha\sigma_{0.5}))$ for lower (a) and higher (b) domains, c) $n\ln(\sinh(\alpha\sigma_{0.5})) - 1000/RT$ and d) $n\ln(\sinh(\alpha\sigma_{0.5})) - \ln Z$ for both domains based on hot compression tests.

For lower domain:

$$Z = \dot{\varepsilon}\exp\left(\frac{1160450}{8.314T}\right) = (8.95\times10^{45})\ln[\sinh(0.003957\sigma)^{8.60}] \quad (9)$$

For higher domain:

$$Z = \dot{\varepsilon}\exp\left(\frac{468318}{8.314T}\right) = (3.22\times10^{15})\ln[\sinh(0.012989\sigma)^{3.69}] \quad (10)$$

In other words, according to γ′ status, the activation energy for a lower domain-containing γ′, is approximately 2.5-times more than that of a higher domain when this phase completely disappears in the matrix (Fig. 7); however, the Q-value at overall conditions is calculated to be 820.26 kJ/mol. As listed in Table 1, the range of Q value is different with the presence of γ phase and without it, 330-490 kJ/mol and 939.1-1400 kJ/mol, respectively, where for γ′-containing superalloys is in the range of 930.1-1400.0 kJ/mol. Furthermore, the alloys with complex conditions of γ′ in the temperature range of deformation i.e., absent at some temperatures and presence at other ones, have Q-value in the range of 691.0-903.6 kJ/mol, as seen in the mentioned table. This behavior can be seen in the hot working of the investigated superalloy at all conditions (Table 1). In other words, the γ′ can essentially change the hot working dominated mechanisms in superalloys at a lower temperature as compared with the higher domain.

3.5. Prediction of flow stress using overall condition

To predict the stress in the studied alloy using both strategies i.e., overall and separated conditions, the following formula was employed derived from the hyperbolic-sine constructive equation:

$$\sigma = \left(\frac{1}{\alpha}\right)[\sinh^{-1}\left(\frac{Z}{A}\right)]^{\left(\frac{1}{n}\right)} \quad (11)$$

For the prediction of flow stress at overall condition; firstly, the material parameters, i.e., α, n, Q, and Ln A at strains of 0.1-0.5 were achieved in a similar manner, as described in section 3.2, and then presented in Fig. 9. Secondly, the 5th order polynomial functions [31] were

Table 1. The Q-parameter of various superalloys along with its initial microstructure (C: Cast, W: Wrought, P.M.: Powder Metallurgy) and condition of γ/ presence (Presence, Absent and Both of them related to of deformation conditions)

No.	Alloy / Initial condition	Temp. (°C)/Strain rate (s^{-1}) During compression test	Condition of γ/ presence	Q (kJ/mol)	Ref
1	Haynes 230 / W	1050-1250 / 0.1-10	Absent	449	[32]
2	GH925 / W	950-1250 / 0.01-10	Absent	393.5	[33]
3	In028 / W	950-1150 / 0.01-30	Absent	388.3	[34]
4	In600 / W	950-1150 / 0.001-10	Absent	330	[35]
5	In625 / W	1000-1200 / 0.01-10	Absent	483.4	[30]
6	In690 / W	950-1200 / 0.001-10	Absent	380.2	[36]
7	In960 / W	1000-1200 / 0.1-10	Absent	490.1	[37]
8	In718 / W	950-1100 / 0.001-1	Absent	467	[19]
9	In718 / W	950-1180 / 0.001-1	Absent	443	[38]
10	In718 / W	950-1100 / 0.001-10	Absent	429.2	[39]
11	BSTMUF601 / W	950-1200 / 0.2-10	Absent	470.5	[40]
12	Niomonic 80A / W	950-1200 / 0.02-20	Absent	424	[41]
13	Ni-Cr-W / C	1000-1200 / 0.001-10	Absent	456	[42]
14	FGH4096 / P.M.	1050-1140 / 0.002-1	Absent	418	[43]
15	U720Li / C	1100-1190 / 0.01-1	Both	691	[44]
16	FGH96 / P.M.	1000-1150 / 0.001-1	Both	693.2	[45]
17	HG4698 / P.M.	950-1150 / 0.001-30	Both	699.2	[46]
18	PM0001 / P.M.	1000-1100 / 0.001-1	Both	903.6	[11]
19	Ni-Cr-Co / P.M.	950-1150 / 0.0003-1	Both	804.8	[47]
21	U720 / W	1100-1150 / 0.001-1	Presence	1152	[23]
22	Waspaloy / W	1060-1140 / 0.001-1 950-1120 / 0.001-1	Absent Presence	462 1400	[22]
23	In939 / C	1000-1050 / 0.001-1 1100-1150 / 0.001-1	Absent Presence	400.5 930.1	[24]
24	Co-Al-W / C	1100-1200 / 0.001-1 950-1050 / 0.001-1	Absent Presence	496.5 1182.5	[21]
25	AD730 / C	950-1200 / 0.001-1 1100-1200 / 0.001-1 950-1050 / 0.001-1	Both Absent Presence	820.26 468.32 1160.45	Present study

passed from each parameter in the following form which is presented in Fig. 9:

$$f(\varepsilon) = a_5\varepsilon^5 + a_4\varepsilon^4 + a_3\varepsilon^3 + a_2\varepsilon^2 + a_1\varepsilon + a_0 \quad (12)$$

In the next step, the predicted flow stress is calculated by Eq. (11). The predicted stresses as well as the experimental data are shown in Fig. 10.

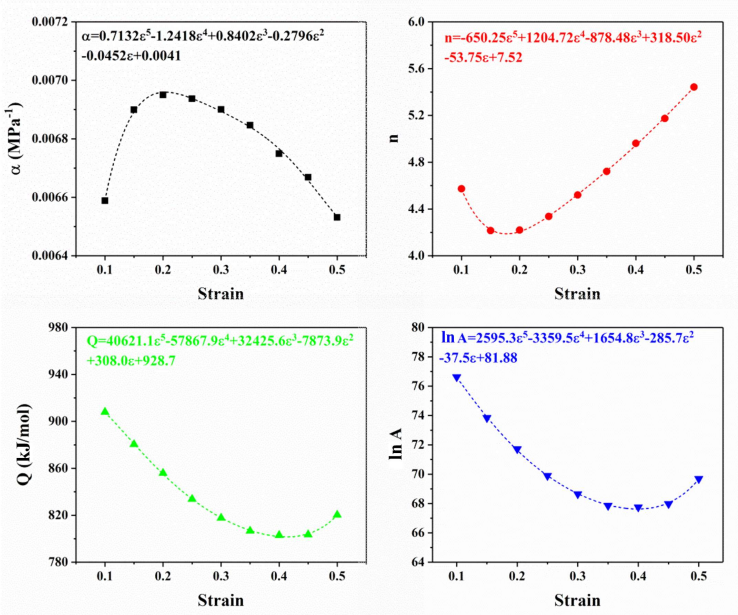

Fig. 9. The variations of hot deformation parameters of hyperbolic sine equation as a function of strain at overall conditions a) α, b) n, c) Q, d) ln A based on hot compression tests at the overall condition.

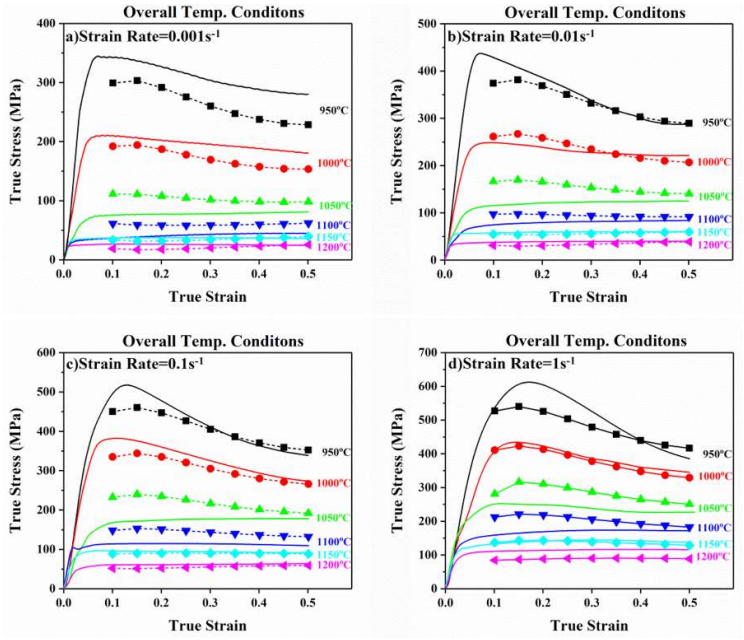

Fig. 10. The prediction stress from hyperbolic sine equation modeling based on overall condition and experimental data at different temperatures and strain rates of a) 0.001 s^{-1}, b) 0.01 s^{-1}, c) 0.1 s^{-1}, and d) 1 s^{-1}.
(solid line and point-dashed curves illustrate experimental and prediction data, respectively).

As can be seen, the predicted stress is perceptibly different from the experimental data, especially in temperatures of 950°C and 1000°C. Similarly, the flow stress prediction is carried out on each separated domain as described above, and then results are presented in Fig. 11. As the results indicate, the predicted stress is approximate to experimental data at all of the temperatures.

To better understand each method, the plots of the experimental data versus the predicted hyperbolic sine

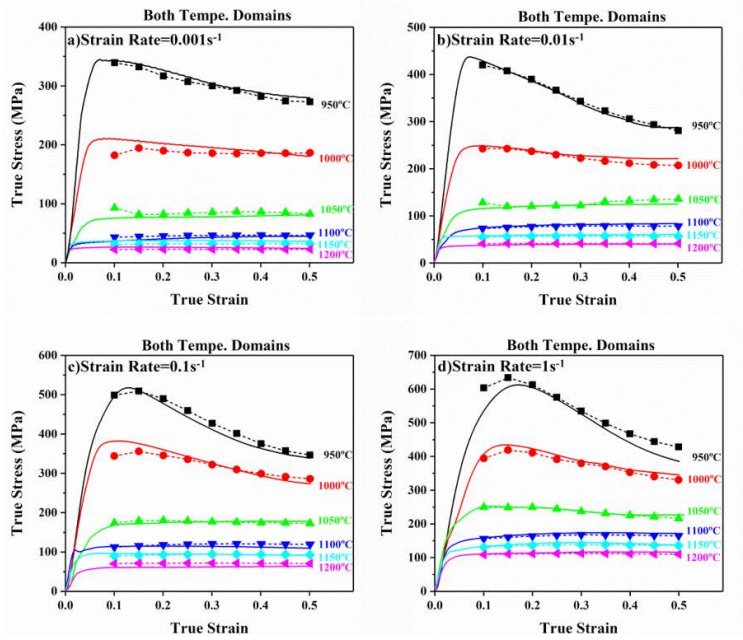

Fig. 11. The prediction stress from hyperbolic sine equation modeling based on separated domains and experimental data at different temperatures and strain rates of a) 0.001 s^{-1}, b) 0.01 s^{-1}, c) 0.1 s^{-1}, and d) 1 s^{-1}.
(solid line and point-dashed curves illustrate experimental and prediction data, respectively).

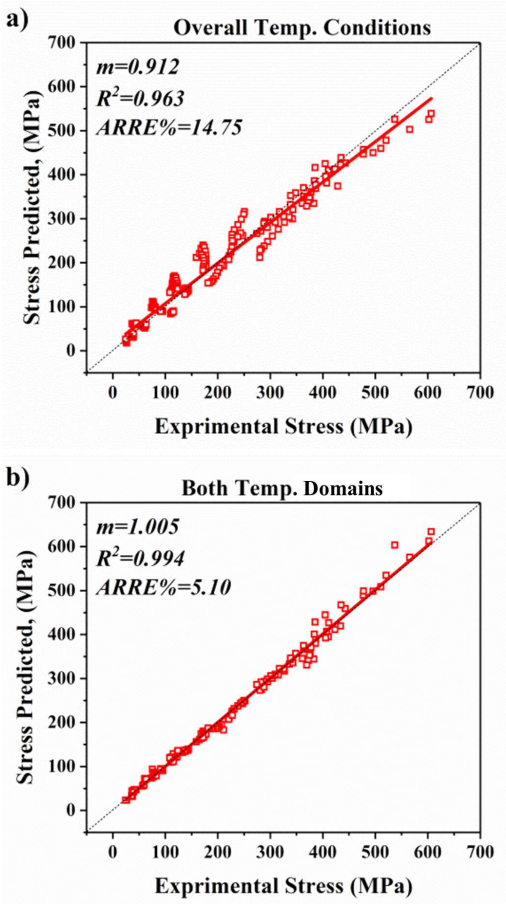

Fig. 12. Correlation between the experimental flow stress and the predicted data by using hyperbolic sine equation.

equation are shown in overall and separated domain manners in Fig. 12. As can be observed, there is a gap in the predicted results with experimental data with two approaches, while this is very narrow for the separated manner. Furthermore, the predictability of two methods is further quantified by employing standard statistical parameters such as correlation coefficient (R) and average absolute relative error (AARE), which are expressed in the following:

$$R = \frac{\sum_{i=1}^{N}(\sigma_{exp.}^{i} - \sigma_{exp.}^{m})(\sigma_{p}^{i} - \sigma_{p}^{m})}{\sqrt{\sum_{i=1}^{N}(\sigma_{exp.}^{i} - \sigma_{exp.}^{m})^2(\sigma_{p}^{i} - \sigma_{p}^{m})^2}} \quad (13)$$

$$AARE = \frac{1}{N}\sum_{i=1}^{N}\left|(\sigma_{exp.}^{i} - \sigma_{p}^{i})/\sigma_{exp.}^{i}\right| \quad (14)$$

where $\sigma_{exp.}^{i}$ is the experimental flow stress, σ_{p}^{i} is the predicted flow stress, $\sigma_{exp.}^{m}$ and $\sigma_{exp.}^{m}$ are the mean values of $\sigma_{exp.}^{i}$ and σ_{p}^{i}, respectively and N is the total number of data. The parameters of R^2 and AARE that are equal to 0.963 and 14.75% for overall condition, these are 0.994 and 5.10% for the separated manner.

According to the predicted results (Fig. 10 and Fig. 11) as well as statistical parameters, it can be stated that a good correlation is obtained by assuming separated deformation domain based on γ'-phase manner; while the model on overall condition presents a relatively poor accuracy for modeling and stress prediction. Furthermore, as indicated in the results, the presented methodology for hot working modeling of AD730, as a γ'-containing alloy, confirms that the hardenable-γ' precipitates can affect the hot deformation behavior, modeling, and stress prediction.

It can be deduced that the governing of classical constitute equation for describing the thermomechanical behavior of a two-phase alloy is quite different with single alloys. The presence of different second phases with dislike interfacial coherency, formability, and volume fraction as well as their size effect can considerably facilitate or postpone useful restoration mechanisms such as DRX while it can stem damaging events like wedge cracking and shear banding. Regardless of interface coherency and intrinsic formability of the second phase, the volume fraction of the studied alloy has to be identified for recognition of the dominant mechanisms in every individual hot deformation regime. When the ratio of phase volume fraction to the phase radius is higher than a specific value (0.2 μm^{-1} [4]), the Zener pinning effect is dominant that prevents DRX facilitation by exerting a retarding force to the grain boundaries. On the other hand, in the case of passing from this specified threshold value, a great deal of energy is focused on a confined area that can act as the potent zone for the nucleation of DRX grains. It is noted that the interaction of such strengthening phases with twin regions can make things quite complex at every hot working condition. For the alloys like AD370, the twin-twin interaction regions, as well as a twin-grain boundary region, may cause a considerable hindering

effect on grain boundaries which may place in the restoration and flow softening after passing the initial work hardening.

4. Conclusions

In the present work, the hot deformation behaviors and modeling of cast-homogenized AD370, as a novel superalloy, were investigated over wide temperature ranges (950ºC-1200ºC) and strain rate (0.001-1 s^{-1}). The effects of hot temperature on flow behavior and microstructural evolution were studied. The following main conclusions can be drawn:

1. Hyperbolic sine constitutive equation at overall condition (950-1200ºC) does not exhibit an ideal correlation between flow stress and deformation parameters based on the following formula:

Overall condition:

$$Z = \dot{\varepsilon}\exp\left(\frac{820259}{8.314T}\right) = (1.83\times10^{30})\ln[\sinh(0.006532\sigma)^{5.44}]$$

2. The DRXed grains were only found at higher temperature domains (1100ºC, 1150ºC, and 1200ºC); whilst, the fact that the deformed microstructure was found at lower temperature ones (950ºC, 1000ºC, and 1050ºC) presented the initial coarse grains as well as the high volume fraction of fine γ′-particles.

3. Based on two separated temperature domains, i.e., lower and higher, the constitutive equation was developed with excellent modeling potential as following:

Lower domain:

$$Z = \dot{\varepsilon}\exp\left(\frac{1160450}{8.314T}\right) = (8.95\times10^{45})\ln[\sinh(0.003957\sigma)^{8.60}]$$

Higher domain:

$$Z = \dot{\varepsilon}\exp\left(\frac{468318}{8.314T}\right) = (3.22\times10^{15})\ln[\sinh(0.012989\sigma)^{3.69}]$$

4. The results indicated that flow stress prediction based on two separated domains can work well in comparison with overall conditions and the γ′-precipitations can play a major factor in modeling and flow prediction in AD730 superalloy.

5. References

[1] R.C. Reed, The superalloys: fundamentals and applications, Cambridge university press, 2008.

[2] M.J. Donachie, S.J. Donachie, Superalloys: a technical guide, ASM international, 2002.

[3] C.T. Sims, N.S. Stoloff, W.C. Hagel, superalloys II, Wiley New York,1987.

[4] F.J. Humphreys, M. Hatherly, Recrystallization and related annealing phenomena, Elsevier, 2012.

[5] R. Doherty, D. Hughes, F. Humphreys, J.J. Jonas, D.J. Jensen, M. Kassner, W. King, T. McNelley, H. McQueen, A. Rollett, Current issues in recrystallization: a review, *Materials Science and Engineering: A*, 238(2) (1997) 219-274.

[6] B. Verlinden, J. Driver, I. Samajdar, R.D. Doherty, Thermo-mechanical processing of metallic materials, Elsevier, 2007.

[7] M. Zeinali, E. Shafiei, R. Hosseini, Kh. Farmanesh, A.R. Soltanipoor, E. Maghsodi, Hot deformation behavior of 17-7 PH stainless steel, *Iranian Journal of Materials Forming*, 4(1) (2016) 1-11.

[8] G.Z. Quan, A. Mao, G.C. Luo, J.T. Liang, D.S. Wu, J. Zhou, Constitutive modeling for the dynamic recrystallization kinetics of as-extruded 3Cr20Ni10W2 heat-resistant alloy based on stress-strain data, *Materials & Design (1980-2015)*, 52 (2013) 98-107.

[9] S. Aliakbari Sani, H. Arabi, S. Kheirandish, G.R. Ebrahimi, flow stress modeling in a γ-γ/ cobalt base superalloy by using the hyperbolic sine equation and ANN Method, *Iranian Journal of Materials Forming*, 6(1) (2019) 44-55.

[10] J. Brooks, Forging of superalloys, *Materials & design*, 21(4) (2000) 297-303.

[11] G. He, F. Liu, J. Si, C. Yang, L. Jiang, Characterization of hot compression behavior of a new HIPed nickel-based P/M superalloy using processing maps, *Materials & Design*, 87 (2015) 256-265.

[12] F. Mohammadi Shore, M. Morakabati, S.M. Abbasi, A. Momeni, Hot Deformation Behavior of Incoloy 901 Through Hot Tensile Testing, *Journal of Materials Engineering and Performance*, 23(4) (2014) 1424-1433.

[13] B. Xie, Y. Ning, C. Zhou, Deformation behavior and microstructure evolution of two typical structures in Udimet 720Li ingot, *Procedia engineering*, 207 (2017) 1093-1098.

[14] F. Liu, J. Chen, J. Dong, M. Zhang, Z. Yao, The hot deformation behaviors of coarse, fine, and mixed grain for

Udimet 720Li superalloy, *Materials Science and Engineering:* A, 651 (2016) 102-115.

[15] N. Bozzolo, N. Souaï, R.E. Logé, Evolution of microstructure and twin density during thermomechanical processing in a γ-γ'nickel-based superalloy, *Acta materialia*, 60(13-14) (2012) 5056-5066.

[16] V. Randle, P. Rios, Y. Hu, Grain growth and twinning in nickel, *Scripta Materialia*, 58(2) (2008) 130-133.

[17] Y.C. Lin, D.G. He, M.S. Chen, X.M. Chen, C.Y. Zhao, X. Ma, Z.L. Long, EBSD analysis of evolution of dynamic recrystallization grains and δ phase in a nickel-based superalloy during hot compressive deformation, *Materials & Design*, 97 (2016) 13-24.

[18] D.X. Wen, Y. Lin, J. Chen, J. Deng, X.M. Chen, J.L. Zhang, M. He, Effects of initial aging time on processing map and microstructures of a nickel-based superalloy, *Materials Science and Engineering: A*, 620 (2015) 319-332.

[19] Y. Wang, W. Shao, L. Zhen, B. Zhang, Hot deformation behavior of delta-processed superalloy 718, *Materials Science and Engineering: A*, 528(7-8) (2011) 3218-3227.

[20] D.X. Wen, Y. Lin, X.H. Li, S.K. Singh, Hot deformation characteristics and dislocation substructure evolution of a nickel-base alloy considering effects of δ phase, *Journal of Alloys and Compounds*, 764 (2018) 1008-1020.

[21] S.A. Sani, H. Arabi, G.R. Ebrahimi, Hot deformation behavior and DRX mechanism in a γ-γ/cobalt-based superalloy, *Materials Science and Engineering: A*, 764 (2019) 138165.

[22] A. Chamanfar, M. Jahazi, J. Gholipour, P. Wanjara, S. Yue, Evolution of flow stress and microstructure during isothermal compression of Waspaloy, *Materials Science and Engineering: A*, 615 (2014) 497-510.

[23] H. Monajati, A. Taheri, M. Jahazi, S. Yue, Deformation characteristics of isothermally forged UDIMET 720 nickel-base superalloy, *Metallurgical and Materials Transactions A*, 36(4) (2005) 895-905.

[24] M. Jahangiri, H. Arabi, S. Boutorabi, High-temperature compression behavior of cast and homogenized IN939 superalloy, *Metallurgical and Materials Transactions A*, 44(4) (2013) 1827-1841.

[25] T. Konkova, S. Rahimi, S. Mironov, T. Baker, Effect of strain level on the evolution of microstructure in a recently developed AD730 nickel-based superalloy during hot forging, *Materials Characterization*, 139 (2018) 437-445.

[26] A. Devaux, B. Picqué, M. Gervais, E. Georges, T. Poulain, P. Héritier, AD730™-A New Nickel-Based Superalloy for High Temperature Engine Rotative Parts, *Superalloys 2012*, (2012) 911-919.

[27] S.A.A. Shams, S. Mirdamadi, S.M. Abbasi, D. Kim, C.S. Lee, Mechanism of martensitic to equiaxed microstructure evolution during hot deformation of a near-alpha Ti alloy, *Metallurgical and Materials Transactions A*, 48(6) (2017) 2979-2992.

[28] S. Medeiros, Y. Prasad, W.G. Frazier, R. Srinivasan, Microstructural modeling of metadynamics recrystallization in hot working of IN 718 superalloy, *Materials Science and Engineering: A*, 293(1) (2000) 198-207.

[29] T.F. Chen, G.P. Tiwari, Y. Iijima, K. Yamauchi, Volume and grain boundary diffusion of chromium in Ni-base Ni-Cr-Fe alloys, *Materials Transactions*, 44(1) (2003) 40-46.

[30] Q. Guo, D. Li, S. Guo, Microstructural models of dynamic recrystallization in hot-deformed Inconel 625 superalloy, *Materials and Manufacturing Processes*, 27(9) (2012) 990-995.

[31] Y. Ning, Z. Yao, X. Liang, Y. Liu, Flow behavior and constitutive model for Ni–20.0 Cr–2.5 Ti–1.5 Nb–1.0 Al superalloy compressed below γ′-transus temperature, *Materials Science and Engineering: A*, 551 (2012) 7-12.

[32] Y. Liu, R. Hu, J. Li, H. Kou, H. Li, H. Chang, H. Fu, Characterization of hot deformation behavior of Haynes230 by using processing maps, *Journal of Materials Processing Technology*, 209(8) (2009) 4020-4026.

[33] Z. Shi, X. Yan, C. Duan, Characterization of hot deformation behavior of GH925 superalloy using constitutive equation, processing map and microstructure observation, *Journal of Alloys and Compounds*, 652 (2015) 30-38.

[34] C. Sun, G. Liu, Q. Zhang, R. Li, L. Wang, Determination of hot deformation behavior and processing maps of IN 028 alloy using isothermal hot compression test, *Materials Science and Engineering: A*, 595 (2014) 92-98.

[35] H.Y. Wu, F.J. Zhu, S.C. Wang, W.R. Wang, C.C. Wang, C.H. Chiu, Hot deformation characteristics and strain-dependent constitutive analysis of Inconel 600 superalloy, *Journal of Materials Science*, 47(9) (2012) 3971-3981.

[36] S. Guo, D. Li, H. Pen, Q. Guo, J. Hu, Hot deformation and processing maps of Inconel 690 superalloy, *Journal of Nuclear Materials*, 410(1-3) (2011) 52-58.

[37] C. Sun, J. Liu, R. Li, Q. Zhang, J. Dong, Constitutive relationship of IN690 superalloy by using uniaxial compression tests, *Rare Metals*, 30(1) (2011) 81-86.

[38] H. Yuan, W. Liu, Effect of the δ phase on the hot deformation behavior of Inconel 718, *Materials Science and Engineering: A*, 408(1-2) (2005) 281-289.

[39] M. Azarbarmas, M. Aghaie-Khafri, J. Cabrera, J. Calvo, Microstructural evolution and constitutive equations of Inconel 718 alloy under quasi-static and quasi-dynamic conditions, *Materials & Design*, 94 (2016) 28-38.

[40] C. Sun, X. Zuo, Y. Xiang, J. Yang, Investigation on hot deformation behavior and hot processing map of BSTMUF601 super-alloy, *Metals*, 6(3) (2016) 70.

[41] S.W. Hwang, K.T. Park, J.S. Kim, C.Y. Kim, Analysis of hot deformation of Nimonic 80a using processing map, *Proceedings of the 23th International Conference on Metallurgy and Materials*, Brno, Czech Republic, 2014.

[42] Y. Liu, R. Hu, J. Li, H. Kou, H. Li, H. Chang, H. Fu, Hot working characteristic of as-cast and homogenized Ni–Cr–W

superalloy, *Materials Science and Engineering: A*, 508(1-2) (2009) 141-147.

[43] Y. Ning, Z. Yao, H. Li, H. Guo, Y. Tao, Y. Zhang, High-temperature deformation behavior of hot isostatically pressed P/M FGH4096 superalloy, *Materials Science and Engineering: A*, 527(4-5) (2010) 961-966.

[44] Q. Yu, Z. Yao, J. Dong, Deformation and recrystallization behavior of a coarse-grain, nickel-base superalloy Udimet720Li ingot material, *Materials Characterization*, 107 (2015) 398-410.

[45] X. Wei, L.W. Zhang, S.D. GU, J.L. Zhang, Hot compressive deformation behavior and microstructure evolution of HIPed FGH96 superalloy, *Transactions of Nonferrous Metals Society of China*, 22(1) (2012) 66-71.

[46] P. Zhang, C. Hu, Q. Zhu, C.G. Ding, H.Y. Qin, Hot compression deformation and constitutive modeling of GH4698 alloy, *Materials & Design (1980-2015)*, 65 (2015) 1153-1160.

[47] K. Wu, G. Liu, B. Hu, F. Li, Y. Zhang, Y. Tao, J. Liu, Characterization of hot deformation behavior of a new Ni–Cr–Co-based P/M superalloy, *Materials characterization*, 61(3) (2010) 330-340.